Journal of Turbulence
Volume 6, No. 12, 2005

Taylor & Francis
Taylor & Francis Group

Spectral vanishing viscosity method for LES: sensitivity to the SVV control parameters

R. PASQUETTI*

Lab. J.-A. Dieudonné, UMR CNRS 6621 & Université de Nice-Sophia Antipolis, Parc Valrose, 06108 Nice Cedex 02, France

Where spectral methods are concerned, the spectral vanishing viscosity (SVV) method offers an interesting way of computing high Reynolds number flows since it allows stabilization of the calculations whilst preserving the exponential rate of convergence of the spectral approximation. Here we first show how to implement the SVV method in an existing Navier–Stokes solver and then investigate the sensitivity of the numerical results to its main characteristic parameters, namely the SVV amplitude and the SVV activation mode, by focusing on the computation of a turbulent wake in a cylinder, embedded in a channel-like domain, at Reynolds number $Re = 3900$.

Keywords: Spectral methods; Spectral vanishing viscosity; Large eddy simulation; Cylinder wake

1. Introduction

The computation of turbulent flows remains an attractive and challenging task not only in various applications, e.g. in engineering flows, geophysical flows, but also for a good understanding of turbulence. The large eddy simulation (LES) approach, largely developed over the last two decades, constitutes a valuable way to compute such flows, especially if a direct numerical simulation (DNS) approach would be too expensive or if the Reynolds-averaged Navier–Stokes (RANS) approach would not be sufficiently accurate.

To simulate only the coherent structures of a flow, the LES approach makes use of a modelling of the so-called sub grid scale (SGS) stress tensor (see e.g. [1–3]). It is then of interest to use high-order methods, especially spectral methods, to avoid any mixing of the SGS modelling contribution and numerical approximation errors, which may be of comparable amplitude as emphasized, for example, in [4, 5]. In these papers, where detailed analyses are provided to separate the modelling and discretization errors, a grid-independent LES is set by increasing the 'resolution ratio' Δ/h (Δ, filter width; h, space step size) but, of course, for given Δ a strongly decreasing h results in a dramatic increase in computational cost. Efficient spectral methods then appear interesting even if low-order methods can in fact take benefit from counteractions between the modelling and discretization errors [6].

To achieve a spectral LES, one can associate an efficient approximation of the SGS tensor and a stabilization technique. In this spirit we have proposed combining an approximate deconvolution method (ADM) [7, 8] (see also [9, 10]) with the spectral vanishing viscosity

*Corresponding author. E-mail: rpas@math.unice.fr

Journal of Turbulence
ISSN: 1468-5248 (online only)
http://www.tandf.co.uk/journals
DOI: 10.1080/14685240500125476

(SVV) method [11, 12]. In the frame of a semi-Lagrangian scheme this has lead us to develop a defiltering–transport–filtering (DTF-SVV) algorithm [13]. The stabilization property of the SVV method results from the introduction of an additional viscous term in the Navier–Stokes equations. Without such an additional term, energy accumulates at the higher frequencies until inducing a divergence of the calculation. However, because it only acts in the high-frequency range, the SVV term allows preservation of the so-called spectral accuracy of spectral methods, i.e. the exponential rate of convergence of the numerical approximation towards the exact solution.

More recently we have made some comparisons between DTF-SVV and SVV results for the turbulent wake of a cylinder inside a channel [14]. It appears that the results obtained when using the SVV method alone were already valuable and may even be superior to those obtained when DTF modelling of the SGS tensor was attempted. One may then ask if a SVV-stabilized DNS (say SVV-LES) could not result in a realistic LES. Such an approach was used for the first time in [15], where a SVV-LES was introduced and applied to the spectral element computation of turbulent channel flows. The formulation of the SVV term was, however, different from ours. Similarly, in this paper we restrict ourselves to the SVV method. A sensitivity study to its control parameters is provided for the turbulent wake of a cylinder. Moreover, some comparisons with the experimental data used in [16, 17], and especially from [18], are also presented.

The paper is organized as follows. In Section 2 we describe the wake flow problem in which we are interested, give some basic elements on the SVV method and then show how the SVV method is implemented in the numerical solver. In Section 3 we focus on a classical benchmark: the wake of a cylinder at Reynolds number $Re = 3900$, as, e.g., in [16, 17, 19], except that our flow is confined in the cross-flow direction. It is satisfying to observe that the dependence on the SVV parameters is rather weak, except in the very near wake, especially when looking at the mean recirculation length behind the cylinder. Moreover, comparisons with the experimental data indicate that the present SVV-LES could constitute a valuable no-SGS model LES approach. Section 4 concludes the paper.

2. Wake flow problem and SVV-stabilized spectral solver

We are interested in the computation of wakes behind obstacles embedded in channel-like geometries. The x-, y- and z-axes correspond to the streamwise, cross-flow and spanwise directions, respectively. The z-direction is assumed homogeneous. The flow is governed by the incompressible Navier–Stokes equations:

$$D_t \boldsymbol{u} = -\nabla p + \frac{1}{Re}\Delta \boldsymbol{u} \tag{1}$$

$$\nabla \cdot \boldsymbol{u} = 0 \tag{2}$$

where $\boldsymbol{u}$ is the velocity, p a pressure term, Re the Reynolds number and $D_t = \partial_t + \boldsymbol{u} \cdot \nabla$ stands for the material derivative.

The main characteristics of the spectral method used to solve this set of equations are as follows (see [14, 20] for more details).

- In time, the scheme is globally of second order and makes use of three steps:
  - (i) an explicit transport step, handled with an OIF (operator integration factor) semi-Lagrangian method [21, 22];
  - (ii) an implicit diffusion step;
  - (iii) a projection step, based on an unique grid '$\mathbb{P}_N - \mathbb{P}_{N-2}$' approximation.

- The approximation in space makes use of:
  - (i) a domain decomposition in the streamwise x-direction with non-overlapping subdomains and conforming meshes;
  - (ii) Fourier expansions in the homogeneous spanwise z-direction;
  - (iii) Chebyshev polynomial expansions in x and y (collocation method).
- The bluff body is modelled by using a 'smoothed penalty technique': a force term is introduced into the Navier–Stokes equations to cancel (approximatively) the velocity field inside the obstacle whose 'characteristic function' is smoothed.
- Parallelization/vectorization: each subdomain is associated to one vectorial processor.

2.1 *The SVV method: background*

The SVV method was introduced in the late 1980s to solve non-linear scalar 1D hyperbolic problems with spectral methods. Fourier expansions were used in the periodic case, investigated in [11], whereas Legendre expansions were used in non-periodic geometries [12]. Further refinements were later carried out (see, e.g., [23, 24]). The main goal of the SVV method is to provide a stable scheme while preserving spectral accuracy, i.e. the exponential rate of convergence of the numerical solution towards the exact solution or, in the case of non-continuous functions, towards its fully converged spectral approximation. The SVV method relies on the idea of adding some artificial viscosity only at the highest frequencies, thus allowing preservation of spectral accuracy.

We introduce the SVV method by following the work of [12], i.e. we consider the non-linear 1D scalar conservation law:

$$\partial_t u + \partial_x(f(u)) = 0 \quad \text{in} \quad \mathbb{R}^+ \times (-1, 1) \tag{3}$$

where $f(u)$ is a non-linear function (e.g. for the Burgers equation $f(u) = u^2/2$) and look for a polynomial approximation $u_N(\cdot, t) \in \mathbb{P}_N(-1, 1)$ (set of polynomials of maximum degree N defined in $(-1, 1)$) of $u(\cdot, t)$, solving in some sense the semi-discrete equation:

$$\partial_t u_N + \partial_x I_N(f(u_N)) = \epsilon_N \partial_x(Q_N(\partial_x u_N)) \tag{4}$$

Here I_N denotes the polynomial interpolation onto $\mathbb{P}_N$, ϵ_N is a $O(1/N)$ coefficient and Q_N is the spectral viscosity operator such that, with L_k denoting the Legendre polynomial of degree k:

$$\forall \phi \qquad \phi = \sum_{k=0}^{\infty} \hat{\phi}_k L_k \qquad Q_N \phi \equiv \sum_{k=0}^{N} \hat{Q}_k \hat{\phi}_k L_k \tag{5}$$

where $\hat{Q}_k = 0$ if $k \leq m_N$ and $0 < \hat{Q}_k \leq 1$ if $m_N < k \leq N$ with, e.g., $m_N = \sqrt{N}$.

The characteristic parameters of the SVV methods are thus the spectral viscosity activation mode m_N and the spectral viscosity amplitude ϵ_N. Note that if l is a characteristic length of the grid, from a scaling argument $\epsilon_N = O(l/2N)$. For the variations of $\hat{Q}_k$ with respect to the mode number k, as in [12] we use: $\hat{Q}_k = \exp[-((N-k)/(m_N-k))^2]$, $m_N < k \leq N$. The variations of $\hat{Q}_k$ for three values of m_N are shown in figure 1.

2.2 *Implementation*

The SVV method is implemented in the implicit diffusion step [14, 20]. At this stage we introduce a SVV-modified Laplacean operator Δ_{SVV}, which combines the viscous term and

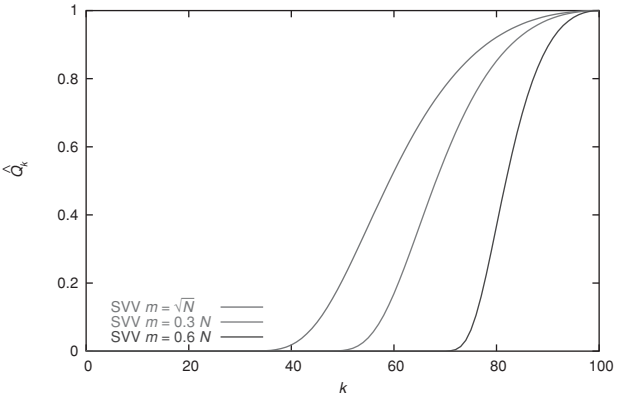

Figure 1. Variations of $\hat{Q}_k$ for $N = 100$ and $m_N = \{\sqrt{N}, 0.3N, 0.6N\}$.

the SVV term. Thus, with a second-order backward Euler approximation of the material derivative and a time-step Δt, the following semi-discrete problem is considered at each time t_{n+1}.

Determine $\boldsymbol{u}^*$ such that:

$$\left(\nu\Delta_{\mathrm{SVV}} - \frac{3}{2\Delta t}\right)\boldsymbol{u}^* = \boldsymbol{f}^{n+1} \quad \text{in } \Omega \tag{6}$$

$$+\,\text{boundary condition, e.g.} \quad \boldsymbol{u}^*|_\Gamma = \boldsymbol{u}^{n+1}|_\Gamma = \boldsymbol{u}_\Gamma$$

with (semi-Lagrangian method and 'Goda scheme' [25]):

$$\boldsymbol{f}^{n+1} = \frac{1}{2\Delta t}(-4\tilde{\boldsymbol{u}}^n + \tilde{\boldsymbol{u}}^{n-1}) + \nabla p^n \tag{7}$$

Here $\boldsymbol{u}^*$ is a provisional (non-solenoidal) velocity and $\tilde{\boldsymbol{u}}^{n+1-q}$, $1 \le q \le 2$, are the velocity at time t_{n+1-q} and at the feet of the characteristics stemming from $(\boldsymbol{x}, t_{n+1})$, in practice at the grid points after space discretization.

To go into the details, let us consider the following scalar elliptic equation:

$$-\nu\Delta u + \alpha_0 u = f \quad \text{in } (-1,1)^2, \qquad 0 < \nu \ll 1, \qquad \alpha_0 \ge 0 \tag{8}$$

The discrete SVV solution u_N should solve, e.g., in the sense of collocation methods:

$$-\nu\Delta u_N + \alpha_0 u_N = f_N + \nabla\cdot\epsilon_N Q_N(\nabla u_N) \tag{9}$$

where one has still to define the term $\epsilon_N Q_N(\nabla u_N)$.

The definition we propose relies on the use of the SVV operator introduced in the 1D case. With N_1 (resp. N_2) the polynomial approximation degree in x (resp. y), it is:

$$\epsilon_N Q_N(\nabla u_N) \equiv \left[\epsilon_{N_1} Q^1_{N_1}(\partial_x u_N), \epsilon_{N_2} Q^2_{N_2}(\partial_y u_N)\right] \tag{10}$$

with $Q^i_{N_i}$ the 1D SVV operator acting in direction i. With such a definition of the operator Q_N, artificial dissipation is effectively provided when required, as discussed in [26]. For more or less different definitions of the spectral viscosity operator in the multidimensional case see [15, 23, 27].

Combining the viscous and SVV terms yields the Δ_{SVV} operator:

$$\Delta_{\mathrm{SVV}} \equiv \nabla\cdot\left(1 + \frac{\epsilon_N}{\nu} Q_N\right)\nabla \tag{11}$$

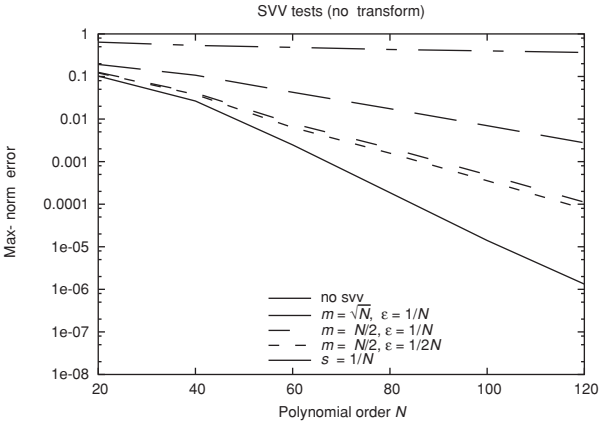

Figure 2. Convergence results for different SVV parameters (m_N, ϵ_N) and also without SVV and with a $O(N^{-1})$ viscous term.

In order to check that the spectral accuracy is preserved, we show in figure 2 some convergence results towards the exact solution: $u_{\text{exact}} = \tanh 30(x^2+y^2-0.25^2)$, when solving the previous elliptic equation with $\nu = 1/900$, $\alpha_0 = 1$ and the appropriate source term. Clearly, introducing a SVV term deteriorates the precision, the best result being obtained without a SVV term. However, the convergence remains exponential and the convergence rate depends on the values of m_N and ϵ_N. Of course, simply adding a $O(N^{-1})$ viscous term only yields a first-order algebraic convergence. Note that the present results were obtained with a Chebyshev collocation method, so that the Chebyshev spectrum was substituted for the Legendre one in the definition of the 1D operator.

The extension to the 3D case with one homogeneous direction is straightforward. For the spanwise z-direction, the 1D SVV operator is defined as in [11] by its action on the Fourier spectrum.

3. LES of the turbulent wake of a cylinder

The characteristic parameters of the computation are the following.

- Reynolds number: $Re = 3900$. The cylinder diameter, the inlet velocity and the ratio of both of them are used for reference length, velocity and time, respectively.
- Computational domain: $\Omega = (-6.5, 17.5) \times (-4, 4) \times (-2, 2)$. The cylinder is of unit diameter and centred at $x = y = 0$.
- Initial conditions: the fluid is at rest ($\boldsymbol{u}_0 = 0$).
- Boundary conditions: free-slip conditions at $y = \pm 4$, unit velocity at $x = -6.5$ (inlet) and 'advection' at the mean flow velocity at $x = 17.5$ (outlet).
- Mesh: number of subdomains: $S = 5$, the interfaces of the subdomains are located at $x = \{-0.5, 2.5, 6.5, 11.5\}$; polynomial approximation degrees in each subdomain: $N_1 = 60$, $N_2 = 120$ in x- and y-directions, respectively; number of Fourier grid points: $N_{\text{F}} = 60$.

Firstly, it should be mentioned that depending on the values of the SVV parameters, the numerical scheme may be unstable. We have not carried out an extensive study but verified that numerical instabilities occur if:

$$m_N \geq 0.7N \text{ when } \epsilon_N = 1/N$$
$$\epsilon_N \leq N/10 \text{ when } m_N = \sqrt{N}$$

Also, it is of interest to mention that a computation was carried out with the much higher Reynolds number $Re = 140\,000$, using $m_N = \sqrt{N}$ and $\epsilon_N = 1/N$. The computation was stable but the mesh seems too coarse or the SVV term too high (with these values of m_N and ϵ_N) to obtain relevant results. They indeed appear to become independent of the Reynolds number, which is meaningful of the fact that the viscous term becomes negligible with respect to the SVV term. Such a problem also arises in standard LESs, when the SGS contribution is too dominant or, say, when the 'subgrid activity parameter' [4, 5] is too high.

The sensitivity to SVV parameters is now addressed. Some comparisons with experimental results are also provided to outline the validity of our numerical results. However, it should be noted that our simulations were carried out in a cross-flow confined geometry and not in the quasi-open domain of the experiments. To study the sensitivity of the numerical results to m_N and ϵ_N, simulations were carried out for $\epsilon_N = 1/N$, $m_N = \{\sqrt{N}, N/3, N/2, 0.6N\}$ and for $m_N = \sqrt{N}$, $\epsilon_N = \{1/N, 1/4N, 4/N\}$. The flow statistics were computed for $t \in (100, 250)$, i.e. during 150 time units from a state where the turbulent flow is well established.

Some qualitative results are presented in figure 3, where isolines of the instantaneous spanwise vorticity in the plane $z = 0$ and at time $t = 150$ are shown. As could be expected, when m_N is increased finer structures are present. On the contrary, when ϵ_N is increased a

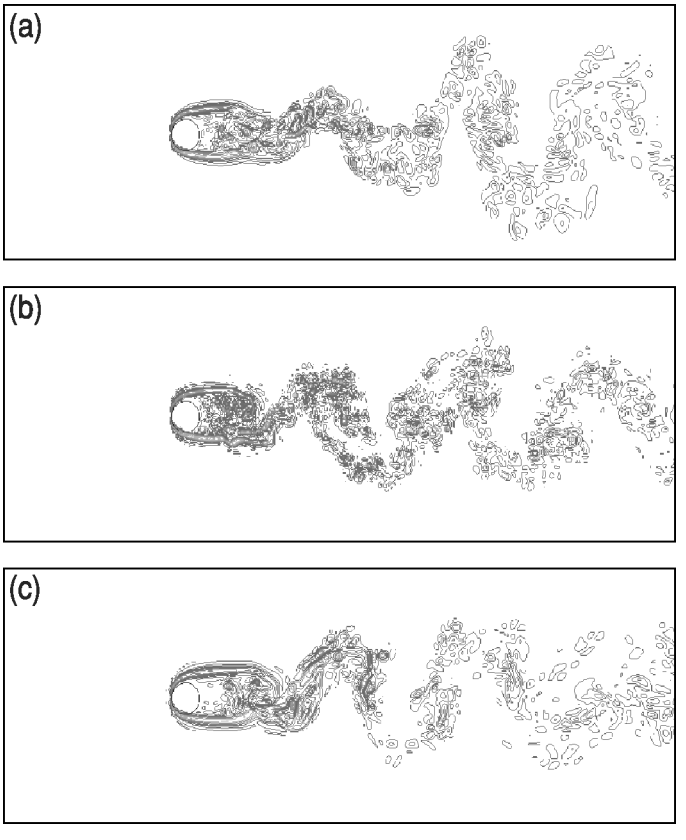

Figure 3. Isolines of the spanwise vorticity in the plane $z = 0$ for (a) $m_N = \sqrt{N}, \epsilon_N = 1/N$ (b) $m_N = N/2, \epsilon_N = 1/N$ and (c) $m_N = \sqrt{N}, \epsilon_N = 4/N$. The visualizations use 30 isolines equidistributed in $(-22, 22)$.

smoothing effect can be observed. The extrema are also slightly different:

$$\text{if } m_N = \sqrt{N}, \epsilon_N = 1/N, \quad \text{then } -27.50 < \omega_z < 22.58$$
$$\text{if } m_N = N/2, \epsilon_N = 1/N, \quad \text{then } -31.69 < \omega_z < 30.82$$
$$\text{if } m_N = \sqrt{N}, \epsilon_N = 4/N, \quad \text{then } -19.69 < \omega_z < 21.64$$

Thanks to the amplification effect of the vorticity one can thus observe some differences in the computed flows: when the SVV term is decreased the flow shows finer vortical structures.

Figure 4 shows the variations of the streamwise, cross-flow and spanwise components of the velocity at a point downstream of the cylinder, in the 'far wake'. One can observe the influence of a variation in m_N (on the left) and the influence of a variation in ϵ_N (on the right). Such history plots may be analysed by providing histograms, i.e. after normalization, estimates of probability density functions (PDFs). Such PDFs are shown in figure 5 for three different values of m_N, with $\epsilon_N = 1/N$, and three different values of ϵ_N, with $m_N = \sqrt{N}$.

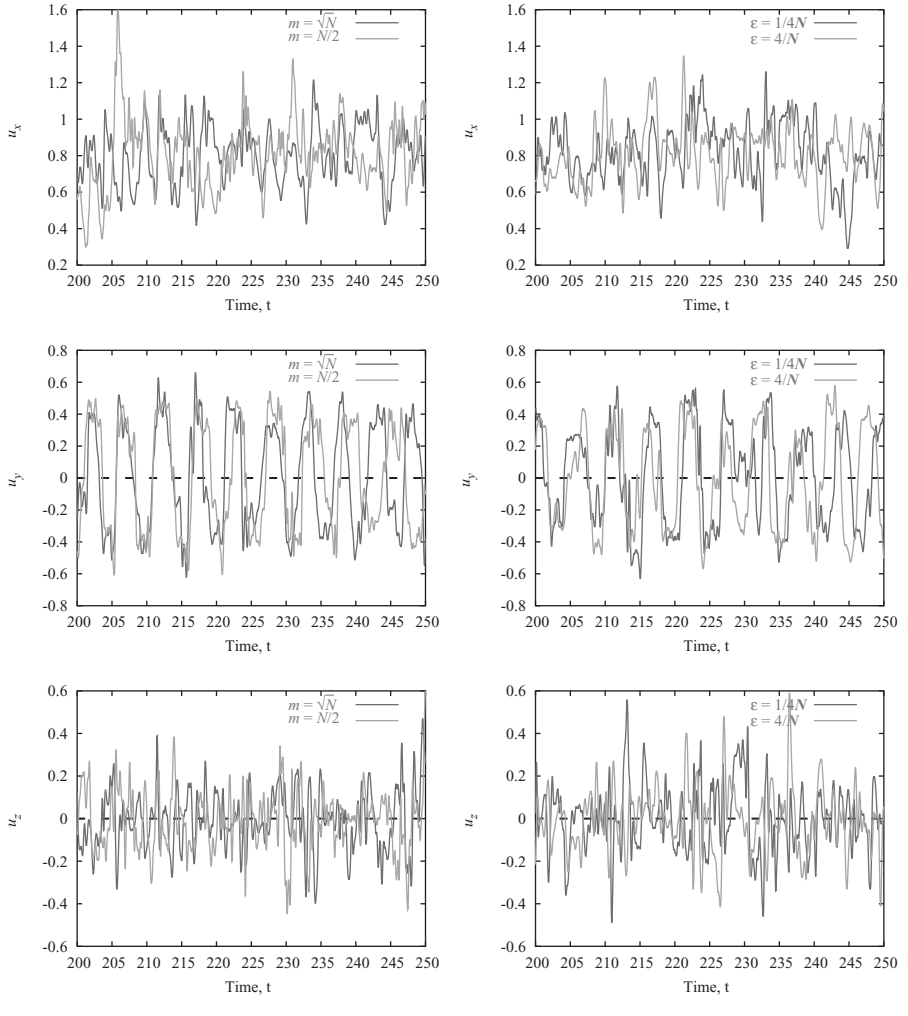

Figure 4. History plots of u_x, u_y and u_z at $P(12.54, 0, 0)$: $m_N = \{\sqrt{N}, N/2\}$, $\epsilon_N = 1/N$ (left); $m_N = \sqrt{N}$, $\epsilon_N = \{1/4N, 4/N\}$ (right).

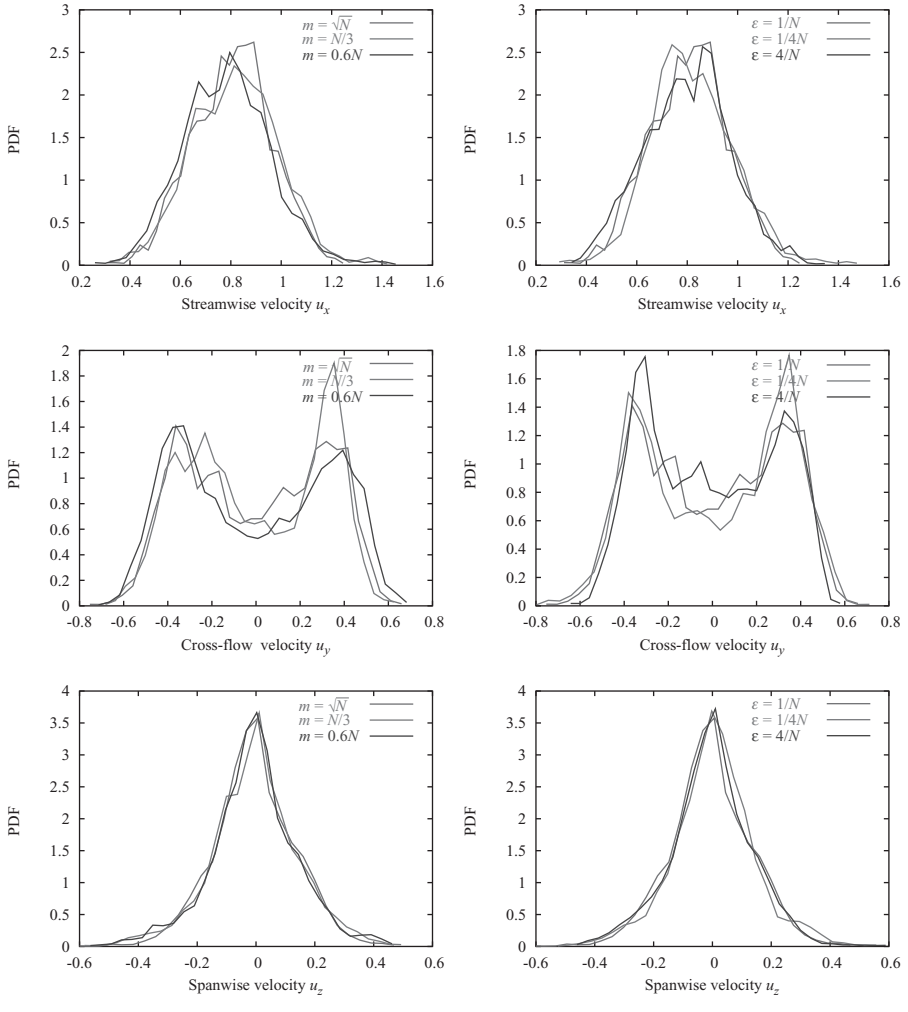

Figure 5. Probability density function of u_x, u_y and u_z at $P(12.54, 0, 0)$: $m_N = \{\sqrt{N}, 0.3N, 0.6N\}$, $\epsilon_N = 1/N$ (left); $m_N = \sqrt{N}$, $\epsilon_N = \{1/N, 1/4N, 4/N\}$ (right).

Although 150 time units were used to compute these PDFs, the time integration appears to be too short, some symmetry properties being still approximative. However, such figures do not show a strong influence of the SVV parameters m_N and ϵ_N.

Via the Taylor hypothesis, the power spectra corresponding to the history plots of figure 4 should be in agreement with Kolmogorov theory ('K41'), i.e. they should show the characteristic $k^{-5/3}$ slope in the inertial range. These power spectra are plotted in figure 6 and compared to the expected slope. To better appreciate the agreement with K41 theory, a standard smoothing based on three frequencies was used. Despite the fact that no SGS tensor modelling is implemented here, one can observe rather good agreement with the K41 theory in about half a decade, as in [16, 17]. Moreover, the sensitivity to the SVV parameters appears weak, although visible in the higher frequency range, which confirms the qualitative observation of the vorticity fields: when decreasing the SVV term amplitude, by increasing m_N or decreasing ϵ_N, one increases the high-frequency content of the power spectra. The Strouhal number, characteristic of the vortex shedding phenomenon, is clearly indicated by the cross-flow component of the

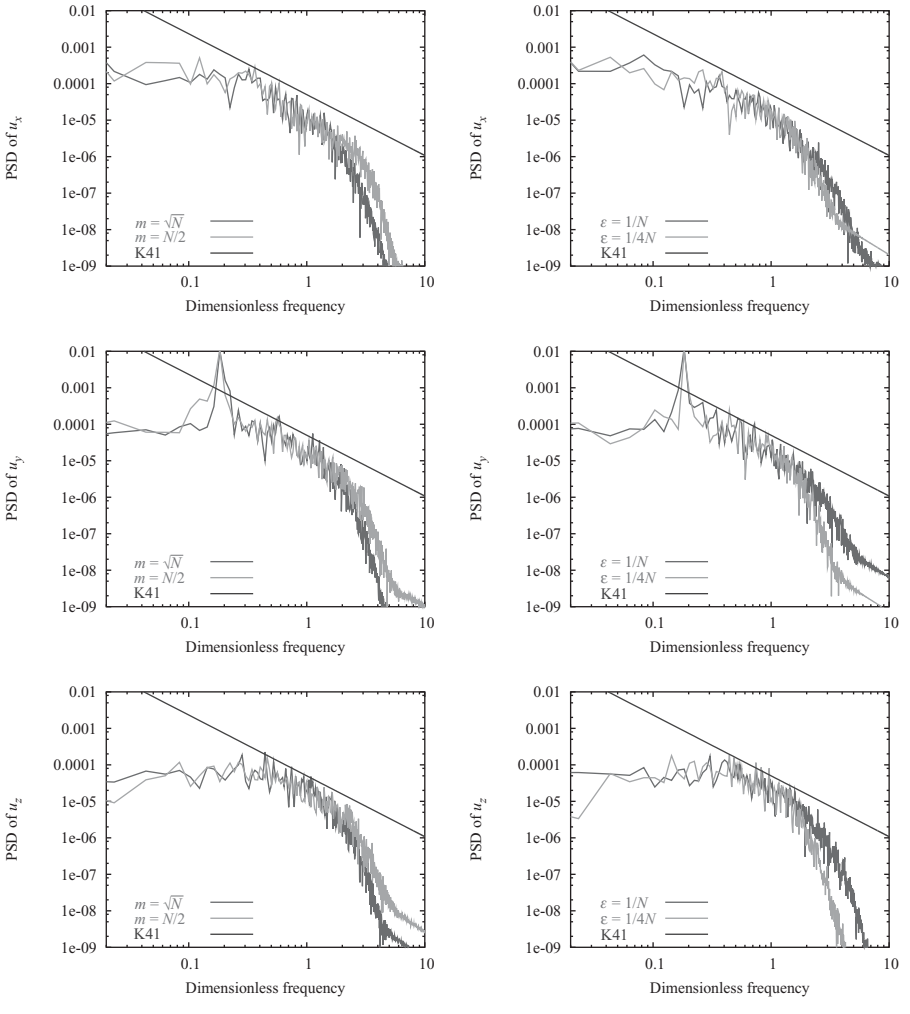

Figure 6. Power spectra of u_x, u_y and u_z at $P(12.54, 0, 0)$: $m_N = \{\sqrt{N}, N/2\}$, $\epsilon_N = 1/N$ (left); $m_N = \sqrt{N}$, $\epsilon_N = \{1/4N, 4/N\}$ (right).

velocity: as expected we find $St \approx 0.2$. The present results are only weakly dependent of the choice of the 'measurement point' as long as this point is located in the fully turbulent part of the wake.

It is also of interest to provide some statistics. Figure 7 shows the mean streamwise velocity $\langle u_x \rangle$, the Reynolds shear stresses $\langle u'^2_x \rangle$ and $\langle u'_x u'_y \rangle$ at $x = 7.36$ (where the prime denotes 'deviation'). Comparisons are provided with the experiments of Ong and Wallace [18]. Although the statistics are not yet well converged for the computations (no averaging in the z-direction, contrary to [16, 17], one can observe some striking similarities with the experimental data, but also some obvious gaps. One can guess that these gaps result from confinement of the simulated flow in the cross-flow direction. This is clear concerning the variation of $\langle u_x \rangle$. Concerning the Reynolds shear stresses, an increase could be expected from the cross-flow confinement, but it would be premature to draw a definitive conclusion. Although the Reynolds shear stresses are not yet converged, as shown by the lack of symmetry of the curves, sensitivity to the SVV parameter values appears again rather weak.

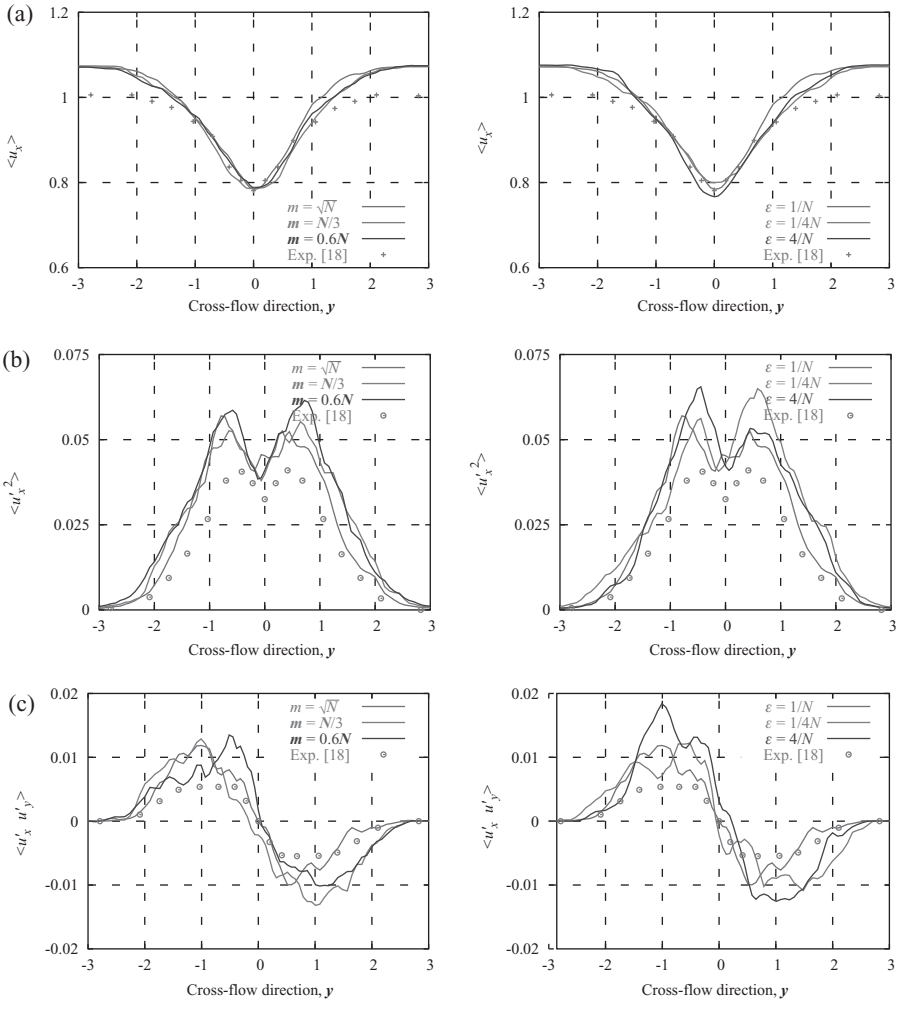

Figure 7. Statistics at $x = 7.36$ ($z = 0$). (a) Mean profile $\langle u_x \rangle$, (b) Reynolds shear stresses $\langle u'^2_x \rangle$ and (c) $\langle u'_x u'_y \rangle$ for $m_N = \{\sqrt{N}, N/3, 0.6N\}$, $\epsilon_N = 1/N$ (left) and $m_N = \sqrt{N}$, $\epsilon_N = \{1/N, 1/4N, 4/N\}$ (right).

However, this weak dependence on the SVV parameters is no longer true in the very near wake, as shown in figure 8 where $\langle u_x \rangle$ and $\langle u'^2_x \rangle$ along the $y = z = 0$ axis are plotted. In particular, the recirculation length behind the cylinder appears sensitive to the SVV parameter values. Clearly, decreasing m_N or increasing ϵ_N, i.e. in both cases increasing the SVV term, results in an increase of the recirculation length. In fact, we note here that the recirculation length is difficult to determine correctly because of its strong dependence on the numerical scheme, on the SGS tensor modelling, on the spanwise length, etc. yielding too low or too high values with respect to the experiments (see e.g. [28]). For the SVV parameters that we have used, the recirculation zone is in our case longer than expected. Moreover, a DTF modelling of the SGS tensor does not improve the situation, as observed in [14]. A possible explanation may still arise here from the cross-flow confinement of the flow. However, as emphasized in [17] there are also great discrepancies of the experimental results in the very near wake, with high sensitivity to upstream disturbances or to the aspect ratio (length/diameter of the cylinder).

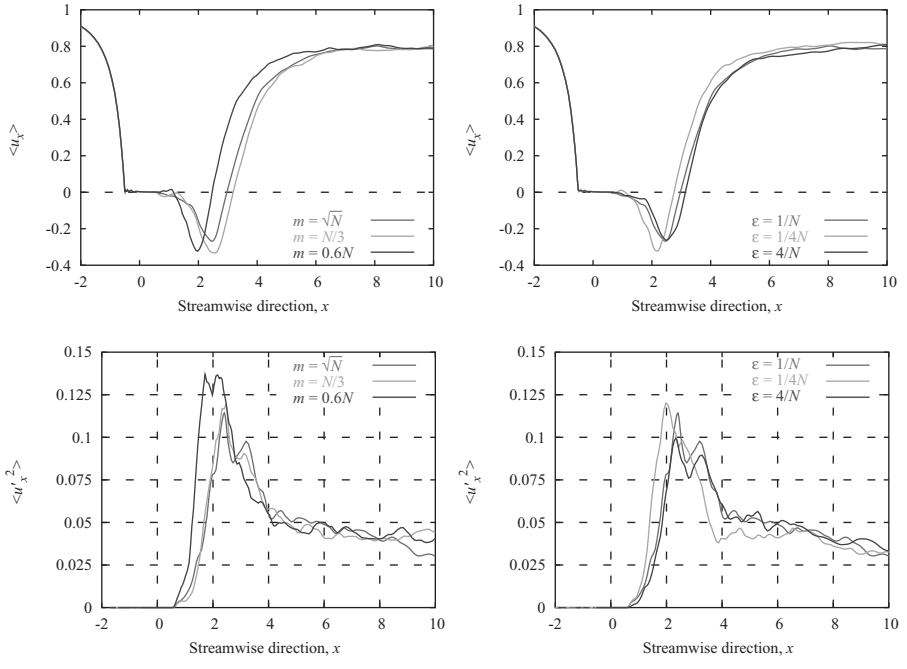

Figure 8. Statistics along $y = z = 0$. Mean profile $\langle u_x \rangle$ and Reynolds shear stress $\langle u'^2_x \rangle$ in streamwise direction: $m_N = \{\sqrt{N}, N/3, 0.6N\}$, $\epsilon_N = 1/N$ (left); $m_N = \sqrt{N}$, $\epsilon_N = \{1/N, 1/4N, 4/N\}$ (right).

Figure 9 compares the numerical result computed for $m_N = 0.6N$ and $\epsilon_N = 1/N$ with the experimental results of Govardhan and Williamson [29] and Lourenco and Shih [30]. Clearly, the flow regimes obtained in the experiments differ, with a smooth or on the contrary a stiff variation of $\langle u_x \rangle$ immediately behind the cylinder. In [17] it is suggested that these differences may result from the different values of the aspect ratio, 10 for Govardhan and Williamson and 20.5 for Lourenco and Shih, but various other experimental details could also explain such a difference (C.H.K. Williamson, private communication). The flow that we have computed is

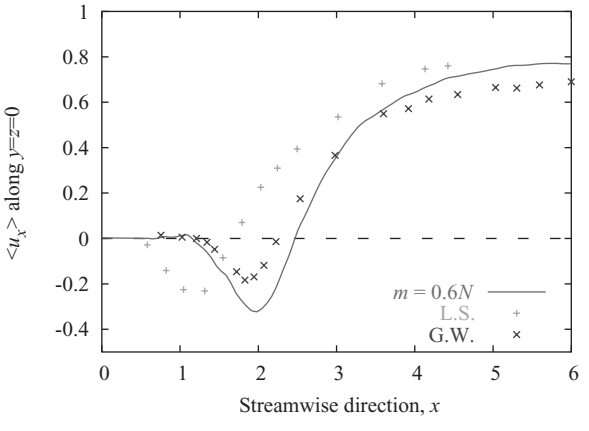

Figure 9. Mean variations of u_x in the streamwise direction. Numerical result obtained with $m_N = 0.6N$ and $\epsilon_N = 1/N$ (solid line); data of Lourenco and Shih [30] (green crosses); data of Govardhan and Williamson [29] (blue crosses).

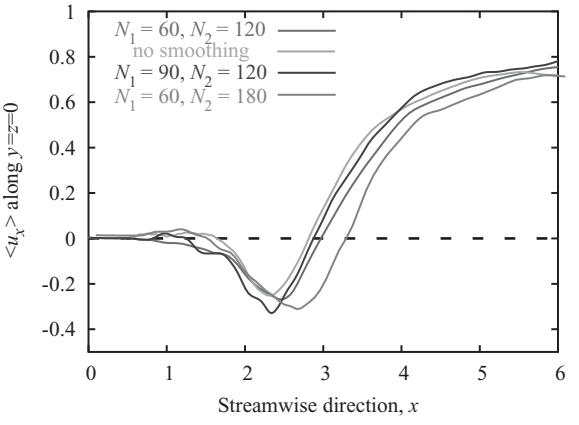

Figure 10. Mean variations of u_x in the streamwise direction for differents meshes and with a non-smoothed penalization; $m_N = \sqrt{N}$ and $\epsilon_N = 1/N$.

close to the experiments of Govardhan and Williamson. On the contrary, the numerical results in [16, 17] are close to the experiments of Lourenco and Shih.

One may ask if the flow regime that we obtained results from some other numerical parameters, e.g. those characteristic of the computational grid. In particular, since a penalty technique was used to model the cylinder, the mesh should be fine enough to describe its boundary correctly. Moreover, we used a 'smoothed' penalty technique: in order to weaken the Gibbs phenomenon the characteristic function of the bluff body is regularized. To check if a different flow regime would be obtained with a refined mesh, we made computations with polynomial approximations different from the one used up to now ($N_1 = 60$, $N_2 = 120$, $N_F = 60$). A computation was thus done with $N_1 = 90$ and another one with $N_2 = 180$, till the final time $t = 150$ (rather than $t = 250$). A calculation was also done with the basic mesh but without regularization of the characteristic function, till the final time $t = 200$. One can observe in figure 10 slight differences in the results, especially for $N_2 = 180$, but these mean profiles are not yet well converged since they were computed on only 50 or 100 time units. In all cases the flow regime is preserved.

4. Conclusion

Where spectral methods are concerned, the SVV stabilization technique appears to be of interest for the LES of turbulent flows. In this spirit a pioneering work was proposed in [15]. The main property of spectral methods is indeed retained: if the exact solution is smooth, the convergence rate of the numerical approximation towards this exact solution is not algebraic, but exponential. Moreover, the SVV method can be implemented in a spectral element solver, opening a way to spectral LES in complex geometries [26].

Using a SVV-stabilized spectral Navier–Stokes solver, we have computed the wake of a cylinder in a channel-like geometry at Reynolds number $Re = 3900$. The Strouhal number was correctly obtained and the power spectra show a good agreement with Kolmogorov theory, decaying at the expected $k^{-5/3}$ slope. Mean profiles of the streamwise component of the velocity and Reynolds shear stresses have also been provided. Such profiles are satisfactory in the far wake but worse in the near wake, the recirculation length behind the cylinder depending on the SVV tuning parameter values. This is, however, not really surprising, when taking into account the large dispersion of the numerical or experimental results.

Because the SVV method does not rely on physical arguments, *a priori* the SVV-LES only constitutes an efficient underlying platform above which a relevant SGS model should be added. This was our initial motivation [13, 14]. However, in the present state-of-the-art of SGS modelling for inhomogeneous and anisotropic flows, the SVV-LES methodology may also be viewed as an interesting no-SGS model spectral LES approach. A nice property is then that DNS results are easily recovered for laminar flows, contrarily to some classical LES techniques. Furthermore, for some academic (and very smooth) flows, SVV-LES results may be more accurate than DNS results, as pointed out in [15, 26] for the 'Kovasznay flow'. Also, the problem of commutation errors between the differentiation and filtering operators no longer arises. Note that the SVV-LES should not be classified as a MILES (monotone integrated large eddy simulation) approach [31]. As the SVV dissipation is explicit it is, e.g., possible to separate the viscous and SVV components of the dissipation rate of turbulent kinetic energy, just as one can separate the viscous and SGS contributions in classical LESs. Some links may be rather found with the multiscale formulation of LES, on the grounds of non-linear Galerkin methods [32], as, for example, described for a Fourier spectral approximation in [33]. Especially, if the 'small scale SGS model' is simply regarded as an *ad hoc* stabilization term, then the analogy is fulfilled. However, in the two-scale formulation there are really two different sets of equations, corresponding to the low and high wavenumbers. This is not the case in the SVV formulation which handles much more smoothly the high-frequency range (see figure 1).

Choosing 'optimal values' of the SVV parameters is not a trivial task, but may be much easier than with the classical LES, since here the aim is not to adjust the parameters of a SGS model. Our best results have been obtained for the largest values of m_N and the smallest values of ϵ_N, the recirculation bubble then being shorter. This is not surprising: bearing in mind that the SVV term was only introduced to stabilize the numerical scheme, it is reasonable to simply minimize its amplitude. Choosing a rather large value of m_N, say $m_N = N/2$, and ϵ_N small, from numerical stability considerations, is from our point of view a good strategy. Moreover, in some specific cases it is also possible to use a strongly anisotropic SVV term, e.g. by activating only some of its components. A dynamic procedure is also possible, but at the price of a higher computational cost, which is presently the same as for a DNS.

Acknowledgments

The computations were made on the NEC-SX5 computer of the IDRIS Computational Center (project 034055). The work was supported by the CNRS, in the frame of the DFG-CNRS project 'Pseudo-spectral methods for LES of complex flows'. We are grateful to G. Darnis (student) and J.M. Lacroix (engineer of the CNRS) for their helpful support.

References

[1] Gatsky, T.B., Hussaini, M.Y., and Lumley, J.L., 1996, Simulation and modelling of turbulent flows. In: J.H. Ferziger (Ed.) *ICASE/LaRC Series in Computational Science and Engineering* Ch. 3, pp. 109–154 (Oxford: Oxford University Press).

[2] Lesieur, M. and Métais, O., 1996, New trends in large-eddy simulation of turbulence. *Annal Review of Fluid Mechanics*, **28**, 45–82.

[3] Sagaut, P., 1998, Introduction à la simulation des grandes échelles pour les écoulements de fluide incompressible. *Mathématiques & Applications* (Berlin: Springer).

[4] Geurts, B.J. and Fröhlich, J. 2002, A framework for predicting accuracy limitations in large-eddy simulation. *Physics of Fluids*, **14**, L41–L44.

[5] Meyers, J., Geurts, B.J. and Baelmans, M., 2003, Database analysis of errors in large-eddy simulation. *Physics of Fluids*, **15**, 2740–2755.

[6] Vreman, B., Geurts, B.J. and Kuerten, H. 1996, Comparison of numerical schemes in large-eddy simulation of the temporal mixing layer. *International Journal for Numerical Methods in Fluids*, **22**, 297–311.
[7] Stolz, S. and Adams, N.A., 1999, An approximate deconvolution procedure for large-eddy simulation. *Physics of Fluids*, **11**, 1699–1701.
[8] Stolz, S., Adams, N.A. and Kleiser, L. 2001, An approximate deconvolution model for large-eddy simulation with application to incompressible wall-bounded flows. *Physics of Fluids*, **13**, 997–1015.
[9] Domaradzki, J.A. and Saiki, E.M., 1997, A subgrid-scale model based on the estimation of unresolved scales of turbulence, *Physics of Fluids*, **9**, 2148–2164.
[10] Geurts, B.J., 1997, Inverse modelling for large-eddy simulation, *Physics of Fluids*, **9**, 3585–3587.
[11] Tadmor, E., 1989, Convergence of spectral methods for nonlinear conservation laws. *SIAM Journal of Numerical Analysis*, **26**, 30–44.
[12] Maday, Y., Kaber, S.M.O. and Tadmor, E., 1993, Legendre pseudo-spectral viscosity method for nonlinear conservation laws. *SIAM Journal of Numerical Analysis*, **30**, 321–342.
[13] Pasquetti, R. and Xu, C.J., 2002, High-order algorithms for large eddy simulation of incompressible flows. *Journal of Sientific Computing*, **17**, 273–284.
[14] Pasquetti, R., 2005, High-order LES modelling of turbulent incompressible flows. *Comptes rendus de l'Académie des Sciences (Mécanique)*, Paris, **333**, 39–49.
[15] Karamanos, G.S. and Karniadakis, G.E., 2000, A spectral vanishing viscosity method for large-eddy simulation. *Journal of Computational Physics*, **163**, 22–50.
[16] Kravchenko, A.G. and Moin, P., 2000, Numerical studies of flow over a circular cylinder at $Re = 3900$. *Physics of Fluids*, **12**, 403–417.
[17] Ma, X., Karamanos, G.S. and Karniadakis, G.E., 2000, Dynamic and low-dimensionality of a turbulent near wake. *Journal of Fluid Mechanics*, **410**, 29–65.
[18] Ong, L. and Wallace, J., 1996, The velocity field of the turbulent very near wake of a circular cylinder. *Experiments in Fluids*, **20**, 441–453.
[19] Fröhlich, J., Rodi, W., Kessler, Ph., Parpais, S., Bertoglio, J.P., and Laurence, D., 1998, Large eddy simulation of flow around circular cylinders on structured and unstructured grids. *Notes on Numerical Fluid Mechanics*, **66**, 319–338.
[20] Cousin, L. and Pasquetti, R., 2004, High-order methods for the simulation of transitional to turbulent wakes. In: Y. Lu *et al.* (Ed.) *Advances in Scientific Computing and applications* (Beijing: Science Press).
[21] Maday, Y., Patera, A.T. and Ronquist, E.M., 1990, An operator-integration-factor splitting method for time-dependent problems: application to incompressible fluid flow. *Journal of Sientific Computing*, **5**, 263–292.
[22] Xu, C.J. and Pasquetti, R., 2001, On the efficiency of semi-implicit and semi-Lagrangian spectral methods for the calculation of incompressible flows. *International Journal for Numerical Methods in Fluids*, **35**, 319–340.
[23] Kaber, O.S.M., 1995, A Legendre pseudo-spectral viscosity method. *Journal of Computational Physics*, **128**, 165–180.
[24] Guo, B., Ma, H., and Tadmor, E., 2001, Spectral vanishing viscosity method for nonlinear conservation laws, SIAM J. Numer. Anal. **39**, 1254–1268.
[25] Goda, K., 1979, A multistep technique with implicit difference schemes for calculation two and three dimensional cavity flows. *Journal of Computational Physics*, **30**, 76–95.
[26] Xu, C.J. and Pasquetti, R., 2004, Stabilized spectral element computations of high Reynolds number incompressible flows. *Journal of Computational Physics*, **196**, 680–704.
[27] Chen, G.Q., Du, Q. and Tadmor, E., 1993, Spectral viscosity approximations to multidimensional scalar conservations laws *Mathematics of Computing*, **204**, 629–643.
[28] Hansen, R.P., and Long, L.N., 2002, Large-eddy simulation of a circular cylinder on unstructured grids. Paper presented at the 40th AIAA Aerospace Sciences meeting, Reno, January 2002, AIAA 2002–0982.
[29] Published in ref. [17].
[30] Published in refs. [16, 17].
[31] Boris, J.P., Grinstein, F.F., Oran, E.S. and Kobe, R.L., 1992, New insights into large eddy simulation, *Fluid Dynamics Research*, **10**, 199–228.
[32] Marion, M. and Temam, R., 1989, Nonlinear Galerkin methods. *SIAM Journal of Numerical Analysis*, **26**, 1139–1157.
[33] Hughes, T.J.R., Mazzei, L. and Oberai, A.A., 2000, The multiscale formulation of large eddy simulation: Decay of homogeneous isotropic turbulence. *Physics of Fluids*, **13**, 505–512.